2024 27th International Conference on Computer and Information Technology (ICCIT)
20-22 December 2024, Cox's Bazar, Bangladesh

Deep Learning Based Lung Image Segmentation Using XR-U-Net

Sajeeb Kumar Ray[1], Ariful Islam[2], Manob Chandra Chanda[3], Naima Islam[4], Md Anwar Hossain[5,*], Mirza A.F.M. Rashidul Hasan[6], and AL AMIN[7]
[1,2,3,4,5,7]*Department of Information and Communication Engineering, Pabna University of Science and Technology, Pabna, Bangladesh*
[6]*Department of Information and Communication Engineering, University of Rajshahi, Rajshahi, Bangladesh*
Email- sajeeb.ray.ice@gmail.com, ariful.210637@s.pust.ac.bd, manob.210624@s.pust.ac.bd, naimaislam204100@gmail.com, manwar.ice@pust.ac.bd, mirzahasanice@gmail.com, alaminabl20110@gmail.com
*Corresponding Author: Md. Anwar Hossain (manwar.ice@pust.ac.bd)

***Abstract*—Lung-associated pathologies are anticipated to emerge as the predominant contributor to mortality rates by the year 2029, as reported by the World Health Organization (WHO). In light of this intensifying issue, we propose an innovative deep-learning framework predicated on the U-Net architecture aimed at enhancing lung segmentation from radiographic imagery. Our proposed model, designated as XR-U-Net, augments the conventional U-Net configuration by integrating five encoder and decoder blocks, which significantly elevates segmentation accuracy to 95.7%. When assessed on a collection of lung X-ray images, the model substantiates its efficacy through critical performance metrics, including validation loss, Intersection over Union (IoU), and Dice coefficient. By reducing diagnostic duration and aiding in intricate medical scenarios, this model possesses considerable potential to assist healthcare practitioners in providing swifter and more precise diagnoses, ultimately addressing the deficiency in the availability of medical specialists.**

Keywords*—*Lung Segmentation, U-Net, Deep Learning, X-ray.

I. INTRODUCTION

One of the most popular and reasonably priced medical imaging methods in the world is X-ray imaging. It is essential in many different types of healthcare environments, from big tertiary hospitals to small community clinics. In particular, chest X-rays are frequently used to identify lung nodules, pulmonary edema, and pneumonia [1]. Chest radiographs are a common diagnostic tool; millions of chest X-rays are taken annually as a result of their effectiveness and accessibility. Chest X-rays are important for routine medical examinations since they make up over one-third of all medical imaging procedures [2].

Chest X-ray lung segmentation poses a number of difficulties because of pathological and non-pathological causes. Accurate segmentation can be hampered by non-pathological abnormalities, such as variations in lung size and shape depending on age, gender, or heart size. Complicating matters is the presence of pathological variables, such as high-intensity opacity brought on by severe lung disorders. Furthermore, a portion of the lung field may be obscured by foreign devices such as catheters, infusion lines, or pacemakers, which makes segmentation much more challenging [3]. The majority of lung segmentation techniques now in use were created using CXR images of either instances with modest lesions or healthy subjects. In order to make sure lung segmentation models are reliable in a variety of clinical scenarios, it is imperative to assess their performance on increasingly difficult and complicated CXR images [4].

Due to advancements in computer image processing and the growing availability of datasets, deep learning technology has advanced significantly in the field of medical image analysis in recent years [5]. To be more precise, deep neural networks are utilized in semantic segmentation to categorize each pixel in a chest radiograph as belonging to the lung area or not. Better outcomes in medical diagnosis have been obtained by this pixel-level categorization, which has increased the accuracy of lung segmentation in chest X-rays [6]. In medical image segmentation, U-Net has become a key architecture, especially for chest X-rays, because of its capacity to generate extremely accurate segmentations [15]. With the help of skip connections and its encoder-decoder structure, it is able to preserve both high-level and low-level characteristics, guaranteeing a thorough comprehension of the context of the images.

In this study, we improved the conventional design, which usually comprises four layers, by using a U-Net architecture with a unique quintuple-layer encoder structure. Without requiring picture preprocessing, this sophisticated arrangement enables more thorough feature extraction, greatly enhancing the precision and caliber of segmentation outcomes. Visual evaluations of the segmented pictures and important performance measures like accuracy, Intersection over Union (IoU), and the dice coefficient are used to show how successful this customized model is. Notably, XR-U-Net's stability and operating efficiency are highlighted by the remarkable results it gets even when trained on smaller datasets.

II. RELATED WORKS

Machine learning (ML) and deep learning (DL) have found widespread uses in medicine, particularly in the identification of conditions like brain tumors, lung nodules, pneumonia, and breast cancer. Deep learning, a subfield of machine learning, has demonstrated promise in improving image segmentation and classification outcomes. As a result, it has become a well-liked method for medical image processing jobs and has acquired substantial support within the scientific community [7].

In order to detect tumors and lung cancer, Brahim et al. [8] showed the usage of a U-Net CNN for lung segmentation from CT scan pictures. With a high-performance Dice score of 0.95, the model demonstrated its ability to separate lung regions appropriately. For segmenting pulmonary parenchyma from CT images, Chen Zhou et al. [9] created an automated segmentation model that combines a spatial transform network (STN) and a 3D V-Net. The model assists radiologists in diagnosing COVID-19 by evaluating texture and data from the segmented areas, enhancing the accuracy and efficacy of the diagnostic process.

Gaal et al. [10] introduced a novel deep-learning method for lung segmentation by fusing a fully convolutional neural network with an adversarial critic model. The remarkable average Dice Coefficient (DC) value of 0.975 on the JSRT dataset confirms the remarkable accuracy of the lung area separation approach they employed. This approach demonstrates using adversarial models to improve medical photo segmentation.

In order to segment the lung areas using an encoder decoder based Fully Convolutional Network (FCN), Rashid et al. [11] used post-processing techniques such as the flood-fill algorithm, unwanted item removal, and morphological alterations. Using their method, the JSRT, MC, and a private dataset produced segmentation accuracies of 0.971, 0.977, and 0.942, respectively. It's interesting to note that every model that has been released can differentiate between non-lung and lung parts by independently acquiring image characteristics.

Feidao Cao [12] improved the feature extraction capabilities of the network by adding a variational autoencoder (VAE) to each encoder-decoder layer in the classic U-Net design. Utilizing both the NIH and JSRT datasets for training and testing, the adjusted network produced accuracy values of 0.9701 and F1 scores of 0.9334 on the former, and accuracy values of 0.9750 and F1 scores of 0.9578 on the latter. This indicates how well the VAE integration improves segmentation performance.

Ngo et al. [13] developed a hybrid methodology that blends deep structured inference with distance regularized level set approaches to present a unique way for lung segmentation in chest X-rays (CXR). On the JSRT dataset, their technique yielded a remarkable average accuracy ranging from 94.8% to 98.5%. This novel method shows how better segmentation accuracy might be achieved in applications involving medical imaging.

A deep learning architecture is described by Rahman et al. [14] with the goal of improving the accuracy of lung region segmentation in Chest X-ray (CXR) images. Using a "divide and conquer" strategy, they segment each of the smaller picture patches that made up the original CXRs before putting them back together to achieve full segmentation. This method combines a modified U-Net architecture for segmentation with a standard Convolutional Neural Network (CNN) for patch classification to yield superior pre-segmented photos through the integration of both models.

Liu et al. [15] describe a dependable and accurate automated lung segmentation method using the U-Net architecture. Their proposed solution adds residual blocks and Leaky ReLU activation functions to an already-trained EfficientNet-B4 encoder, thereby improving the decoder's performance. Their method produces impressive results: on the JSRT and MC datasets, their Jaccard Index scores are 95.8% and 95.5%, respectively.

In order to improve the U-Net model for dense pancreatic segmentation from CT images, Ozan Oktay et al. [16] included attention gates. By efficiently suppressing unnecessary portions within the pictures, these attention coefficients increase the focus and capacity of the model without the need for additional modules. By focusing on the CT scan areas that are most pertinent, this method maximizes segmentation.

Olaf Ronneberger et al. [17] introduced the U-Net segmentation model. It was trained by assigning a class label to every pixel for three biological activities. To enhance the segmentation accuracy, the training images underwent elastic deformations. The model's skip connections combine local data and up-sampled feature maps to guarantee more precise segmentations and improve the localization process overall. Applying the U-Net design, Rehman et al. [18] were able to get a mean Intersection over Union (mean IoU) score of 92.82% while creating lung segmentations from X-ray images. This shows that U-Net is a dependable technique for lung image processing in medical diagnostics by effectively segmenting lung areas from chest radiographs.

Even though lung segmentation techniques have advanced significantly, the majority of current methods struggle to handle complicated chest X-rays with overlapping structures, severe disease changes, and foreign objects. Furthermore, even if U-Net and its variations have demonstrated impressive potential, feature extraction and segmentation accuracy can still be enhanced, especially when dealing with smaller or more varied datasets. In order to improve feature extraction without preprocessing and guarantee excellent segmentation accuracy and resilience across a range of clinical settings, this work presents a unique U-Net architecture with a quintuple-layer encoder structure. Our suggested method seeks to close these gaps and establish a new standard for lung segmentation from chest X-rays.

III. Materials and Method

A. Experimental Design

In order to optimize computational capabilities for our endeavors, we have opted for the Kaggle environment, which employs a GPU P-100 equipped with 64GB of RAM in a cloud infrastructure, supplemented by CPU resources as a contingency. Fig. 1 shows the workflow diagram for lung image segmentation using the XR-U-Net model. This flowchart describes the sequential steps involved in the model's operation, from input data collecting to final output development.

The procedure's initiation starts with the collection of the dataset. Following that, the lung CXR pictures and their corresponding masks are divided into three distinct subsets: the test set, the validation set, and the training set. This partitioning ensures a thorough training program and makes accurate model evaluation easier. During the training and validation phase, the model acquires the capability to segment the lung regions proficiently, utilizing the supplied input data. Upon completion of the model training, the test subsets of both masks and lung CXR images are subjected to the trained XR-U-Net model. This process culminates in the generation of the final output, comprising segmented masks that accurately depict the lung regions.

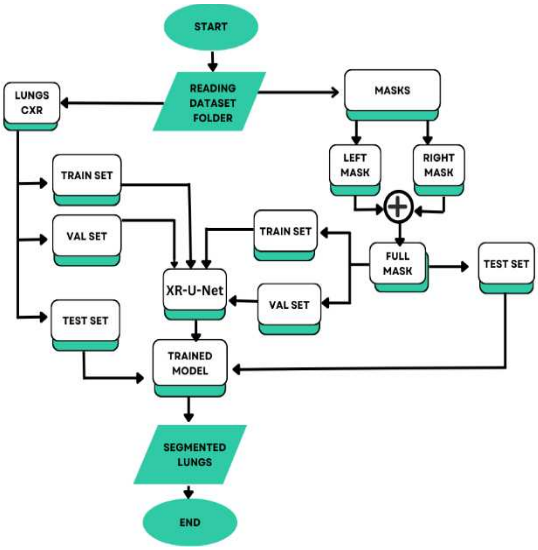

Fig. 1. Workflow diagram of lung image segmentation using XR-U-Net.

B. Dataset

The X-ray pictures included in this data set were obtained from the Department of Health and Human Services' tuberculosis control program in Montgomery County, Maryland, USA [19]. There are 138 posterior-anterior X-rays in this collection; 80 of them are normal, while the remaining 58 show abnormalities consistent with tuberculosis. All photos are in DICOM format and have been de-identified. The set includes several different anomalies such as miliary patterns and effusions. Fig. 2 shows sample photos from this dataset.

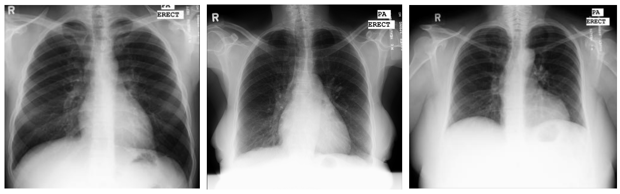

Fig. 2. Sample images from the dataset.

Three distinct subsets of the dataset—training, validation, and testing—were randomly selected. The training subset comprised 112 images, the validation subset encompassed 13 images, while the residual 13 images were designated for the testing subset.

C. Maintaining the Integrity of the Specifications

This section presents a unique deep learning-based lung segmentation method using the XR-U-Net architecture on chest X-ray (CXR) images. The sections that follow provide specifics about the dataset that was used to train the model. Fig. 3 shows the architecture of the suggested model. Each of the five blocks that make up the XR-U-Net encoder is in charge of converting the input data into feature representations. Every encoder block consists of a max pooling layer after a Conv_Block. Two convolutional layers, batch normalization, and ReLU activation make up the Conv_Block.

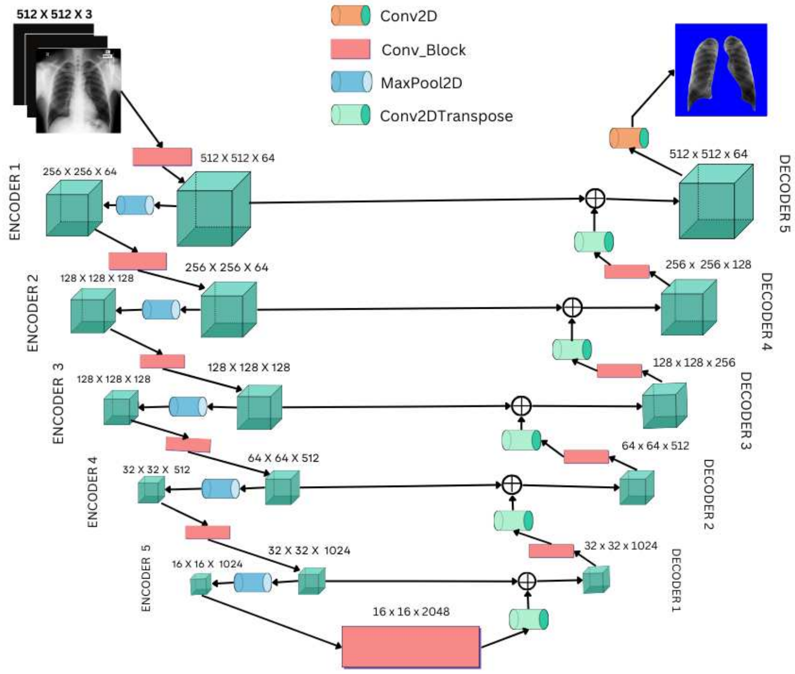

Fig. 3. System architecture of XR-U-Net.

The max pool is defined by the equation (1),

$$\sigma 1(x^L) = \max\left(0, x^L_{i,c}\right) \quad (1)$$

Where ${x^L}_{i,c}$ is the layer L feature map with its i-pixel position, C channel dimensions, and feature activations that can be expressed using the format provided by equation (2).

$$x^L_c = \sigma 1\left(\sum_{c' \in F_L} x^{L-1}_{c'} * k_{c',c}\right) \quad (2)$$

where F_L is the feature map at layer L and $*$ is the convolution operation.

Following the encoding phase, the dimensions of the features are shrunk to 16x16x1024. The decoding stage comes next, with another Conv_Block added at this point. Five blocks make up the decoder, and they all use the Conv2DTranspose operation.

D. Training

We introduced an innovative segmentation architecture, referred to as XR-U-Net, which produces outputs that differentiate lung regions from non-lung regions. The Adam optimizer was utilized to optimize the model, with a learning rate of 1×10^{-6}, with batch size 2. The training process continued for 100 epochs. The optimizer equation (3) is given below:

$$w_t = w_{t-1} - \eta \frac{\hat{m}_t}{\sqrt{\hat{v}_t}+\varepsilon} \quad (3)$$

where w speaks to the weight, η is the learning rate, and epsilon may be a little constant presented to anticipate division by zero. This detailing permits Adam to adaptively alter the learning rate for each parameter based on the gauges of to begin with and moment minutes of the angles, coming about in progressed meetings and execution amid the preparing prepare.

With this setup, the model was able to be trained and validated on the Montgomery County X-ray dataset quickly and effectively. When analyzing the training graph illustrated in Fig. 4 and Fig. 5, where only improved training values are included. It becomes evident that the XR-U-Net model has performed exceptionally well. This is particularly clear from the Dice coefficient and the Intersection over Union (IoU) values, both of the curve approaches towards 1, indicating a high degree of accuracy in the segmentation.

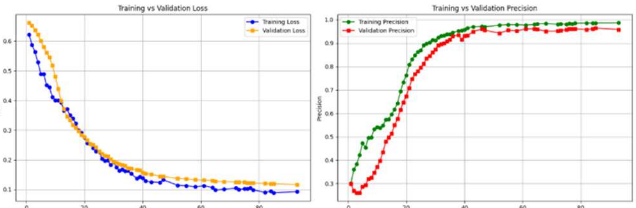

Fig. 4. Training graph, the left side presents the training vs validation loss curve and the right side presents the training vs validation precision graph.

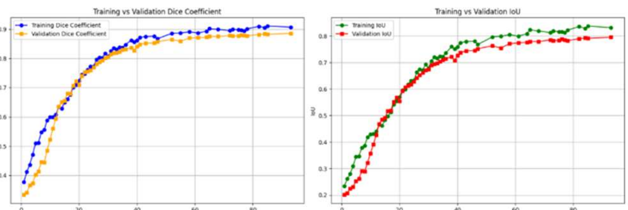

Fig. 5. Training graph, the left side presents the training vs validation dice coefficient curve and the right side presents the training vs validation IoU graph.

The formula to calculate IoU is illustrated in equation (4) and the formula for the dice coefficient is shown in equation (5).

$$IoU = \frac{Area\ of\ Itersection(A \cap B)}{Area\ of\ Union(A \cup B)} \quad (4)$$

The lung parenchyma area, S, is determined by the suggested model, while T represents the ground truth that is achieved through manual segmentation.

$$dsc = 2 * \frac{||S \cap T||}{||S \oplus T||} \quad (5)$$

Where Area of Intersection = Common area shared by the two masks

Area of Union = Total area covered by the two masks

Furthermore, the validation loss shows a steady decline, indicating that the model is robust in precisely segmenting lung areas and that it can generalize well to new data.

IV. Results and Discussion

The XR-U-Net architecture elucidated in this investigation proficiently generated masks for the inputted lung radiographic images, attaining a remarkable accuracy rate of 95.7%. Throughout the training epoch, the model exhibited significant performance metrics, achieving a precision of 98.74%, an Intersection over Union (IoU) score of 0.83, and a Dice score of 0.91. In the validation phase, the model similarly demonstrated robust outcomes, with a precision of 95.73%, an IoU score of 0.79, and a Dice score of 0.88. The masks produced distinctly delineate the pulmonary regions in a monochromatic black shade, while the non-pulmonary areas are represented in an understated gray, thereby augmenting the clarity of the differentiation between the two regions. This discernment serves as an affirmation of the model's adeptness in precisely identifying the anatomical structures of the lungs with exceptional accuracy.

A number of models have been compared with our proposed XR-U-Net illustrates in Table 1. The Fully Convolutional Neural Network (FCNN) developed by Kumar et al. [20] attains a commendable accuracy of 97%; however, the omission of reported Intersection over Union (IoU) and Dice Coefficient metrics renders the model's segmentation efficacy ambiguous. Likewise, the assessment conducted by Boodi et al. [21], which utilized a U-Net architecture in conjunction with a bespoke dataset, raises issues regarding comprehensiveness, as they document a high Dice Coefficient (95%) while failing to delineate the IoU, a pivotal metric for evaluating segmentation capability. The convolutional neural network-based methodology presented by Pasa et al. [22] exhibits a relatively subpar accuracy of 86.6%, highlighting its inadequacies in effectively addressing segmentation tasks.

Conversely, Mique et al. [23] harnessed a Deep Residual U-Net, attaining an extraordinary Dice Coefficient of 98.6% within a mere 40 epochs. Nonetheless, such expedited convergence may suggest a propensity for overfitting attributable to insufficient training. Utilizing the identical dataset as this investigation, Gite et al. [24] implemented U-Net++, achieving enhanced accuracy of 98% and a Dice Coefficient of 97.96%. However, this improvement is accompanied by a substantial increase in model complexity, resulting in prolonged execution times and elevated computational requirements, thereby constraining its applicability in practical scenarios. In contrast, the proposed XR-U-Net achieves an equilibrium between performance and efficiency, providing a competitive accuracy of 95.7% and a Dice Coefficient of 91% with streamlined execution and diminished computational overhead, rendering it more conducive for practical deployment.

The XR-U-Net model proposed herein successfully generated masks for the input lung X-ray images. These masks delineate the lung regions in black while representing the non-lung areas in gray, thereby facilitating a clear differentiation between the two areas. This differentiation exemplifies that the model has effectively developed the capability to identify the anatomical configuration of the lungs. The masks produced by the model, which distinctly segment the lung regions, are illustrated in Fig. 6.

TABLE I. COMPARISON OF SEGMENTATION PERFORMANCE METRICS ACROSS VARIOUS MODELS

Reference	Method	Dataset	Epoch	IoU	Dice	Accuracy
Kumar et al. [20]	FCNN	JSRT	50	Not specified	Not specified	97%
Boodi et al. [21]	U-Net	Custom	Not specified	Not specified	95%	98%
Pasa et al. [22]	CNN	Custom	Not specified	Not specified	Not specified	86.6 %
Mique et al. [23]	Deep Residual U-Net	Not specified	40	Not specified	98.60 %	Not specified
Gite et al. [24]	U-Net++	Montgomery County X-ray Set	Not specified	0.95	97.96 %	98 %
Proposed	**XR-U-Net**	**Montgomery County X-ray Set**	**100**	**0.83**	**91 %**	**95.7 %**

Despite potential noise or distortions present in the X-ray images, the masks maintain a clear and consistent distinction between the lung regions and the surrounding tissues, thereby indicating the model's proficiency in detecting lung parenchyma.

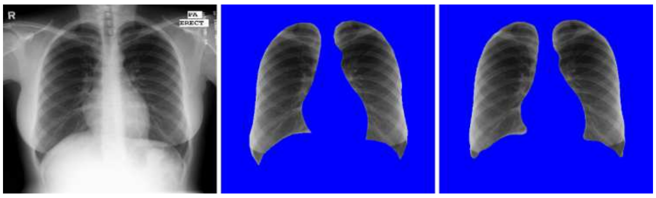

(a) (b) (c)

Fig. 6. Lung CXR images a) input image b) ground truth segment, and c) predicted segment

The XR-U-Net model produced augmented visual outputs alongside mask outputs, facilitating a more straightforward comparison between the projected lung borders and the ground truth segmentations. The definitive lung boundaries are represented by a red border, whereas the predicted lung segments are highlighted with a blue border. The capacity to directly juxtapose these color-coded representations elucidates the accuracy of the algorithm in forecasting lung edges. Illustrations of these bordered outputs are presented in Fig. 7. The lung regions predicted by the model are represented by the blue borders, whereas the ground truth annotations are illustrated by the red borders. The significant overlap between the two, as evidenced in the images, showcases the model's remarkable proficiency in accurately segmenting the lung regions. Although certain intricate structures exhibited minor discrepancies, overall.

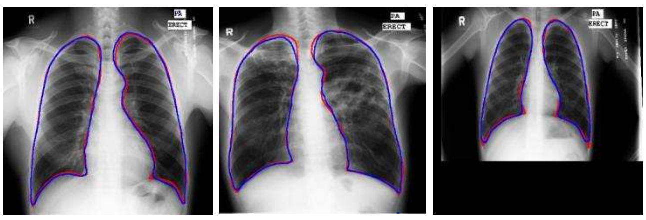

Fig. 7. Examples of segmentation results. The red border indicates the ground truth whereas the green border indicates our prediction masks.

Although the XR-U-Net model demonstrates encouraging outcomes, a critical limitation of this inquiry is the inadequacy of sufficiently comprehensive and varied datasets, which are essential for enhancing the model's resilience and applicability. In subsequent investigations, scholars ought to delve into three-dimensional image segmentation methodologies, which may yield a more holistic comprehension of pulmonary anatomy. Furthermore, the amalgamation of this methodology with effective lung cancer detection frameworks possesses considerable promise for enhancing early diagnostic procedures and treatment efficacy.

V. CONCLUSION

The XR-U-Net model attains a commendable accuracy rate of 95.7%, a Dice coefficient of 91%, and an Intersection over Union (IoU) of 0.83 in the segmentation of lung structures from chest X-ray images. Its innovative quintuple-layer encoder-decoder architecture proficiently manages intricate lung anatomies and associated pathologies, thereby providing a computationally efficient framework suitable for clinical utilization. Upon evaluation using the Montgomery County X-ray dataset, the model reliably delineates pulmonary regions, thereby facilitating precise and expedient diagnostic outcomes.

Despite its promising capabilities, the generalizability of the model would be enhanced through the incorporation of larger and more heterogeneous datasets. Subsequent investigations should prioritize the exploration of three-dimensional segmentation techniques as well as their integration with diagnostic frameworks to augment the early detection of pulmonary diseases. The XR-U-Net model exhibits substantial potential for optimizing diagnostic workflows and improving patient outcomes in response to the escalating prevalence of lung-related pathologies.

ACKNOWLEDGMENT

We gratefully acknowledge the support and resources provided by the Department of Information and Communication Engineering (ICE) at Pabna University of Science and Technology (PUST) for this research. This project was made possible through funding from the ICE Research Fund, PUST.

REFERENCES

[1] B. Van Ginneken, B. T. H. Romeny, and M. A. Viergever, "Computer-aided diagnosis in chest radiography: a survey," IEEE Transactions on Medical Imaging, vol. 20, no. 12, pp. 1228-1241, 2001.

[2] C. Ridge, A. McErlean, and M. Ginsberg, "Epidemiology of Lung Cancer," Seminars in Interventional Radiology, vol. 30, no. 2, pp. 93–98, May 2013.

[3] S. Candemir, S. Antani, and A. Jaeger, "A review on lung boundary detection in chest X-rays," International Journal of Computer Assisted Radiology and Surgery, 2019. doi: 10.1007/s11548-019-01917-1.

[4] B. Van Ginneken, M. B. Stegmann, and M. Loog, "Segmentation of anatomical structures in chest radiographs using supervised methods: a comparative study on a public database," Medical Image Analysis, vol. 10, pp. 19–40, 2006. doi: 10.1016/j.media.2005.02.002.

[5] C. Qin, D. Yao, Y. Shi, and Z. Song, "Computer-aided detection in chest radiography based on artificial intelligence: A survey," BioMedical Engineering Online, vol. 17, p. 113, 2018. doi: 10.1186/s12938-018-0544-y.

[6] H. Greenspan, B. Van Ginneken, and R. M. Summers, "Guest editorial deep learning in medical imaging: Overview and future promise of an exciting new technique," IEEE Transactions on Medical Imaging, vol. 35, pp. 1153–1159, 2016. doi: 10.1109/TMI.2016.2553401.

[7] A. Krizhevsky, I. Sutskever, and G. E. Hinton, "Imagenet classification with deep convolutional neural networks," in Advances in Neural Information Processing Systems (NIPS), 2012, pp. 1097–1105.

[8] B. Ait Skourt, A. El Hassani, and A. Majda, "Lung CT Image Segmentation Using Deep Neural Networks," Procedia Computer Science, vol. 127, pp. 109-133, 2018. doi: 10.1016/j.procs.2018.01.061.

[9] C. Zhao et al., "Lung segmentation and automatic detection of COVID-19 using radiomic features from chest CT images," Pattern Recognition, vol. 119, p. 108071, 2021. doi: 10.1016/j.patcog.2021.108071.

[10] G. Gaál, B. Maga, and A. Lukács, "Attention U-Net based adversarial architectures for chest X-ray lung segmentation," arXiv preprint, arXiv:2003.10304, 2020.

[11] R. Rashid, M. U. Akram, and T. Hassan, "Fully convolutional neural network for lungs segmentation from chest X-rays," in International Conference on Image Analysis and Recognition, 2018, pp. 71-80, Springer.

[12] F. Cao and H. Zhao, "Automatic lung segmentation algorithm on chest X-ray images based on fusion variational auto-encoder and three-terminal attention mechanism," Symmetry, vol. 13, no. 5, p. 814, 2021. doi: 10.3390/sym13050814.

[13] T. A. Ngo and G. Carneiro, "Lung segmentation in chest radiographs using distance regularized level set and deep-structured learning and inference," in IEEE International Conference on Image Processing, 2015, pp. 2140–2143. doi: 10.1109/ICIP.2015.7351179.

[14] M. F. Rahman et al., "Improving lung region segmentation accuracy in chest X-ray images using a two-model deep learning ensemble approach," Journal of Visual Communication and Image Representation, vol. 85, p. 103521, 2022. doi: 10.1016/j.jvcir.2022.103521.

[15] W. Liu et al., "Automatic lung segmentation in chest X-ray images using improved U-Net," Scientific Reports, vol. 12, no. 1, p. 8649, May 2022. doi: 10.1038/s41598-022-12743-y.

[16] O. Oktay et al., "Attention U-Net: Learning where to look for the pancreas," arXiv preprint, arXiv:1804.03999, 2018.

[17] O. Ronneberger, P. Fischer, and T. Brox, "U-Net: Convolutional networks for biomedical image segmentation," in Medical Image Computing and Computer-Assisted Intervention (MICCAI) 2015: Proceedings, Part III, Springer, 2015, pp. 234–241.

[18] T. Rahman et al., "Reliable tuberculosis detection using chest X-ray with deep learning, segmentation, and visualization," IEEE Access, vol. 8, pp. 191586–191601, 2020. doi: 10.1109/ACCESS.2020.3031384.

[19] S. Jaeger et al., "Automatic tuberculosis screening using chest radiographs," IEEE Transactions on Medical Imaging, vol. 33, no. 2, pp. 233-245, Feb. 2014. doi: 10.1109/TMI.2013.2284099.

[20] P. Kumar, P. K. Soni, and L. Raja, "Enhanced Lung Segmentation from Chest X-Ray Images using Attention Based FCNN," International Journal of Intelligent Systems and Applications in Engineering, vol. 12, no. 3, pp. 437–444, 2024.

[21] D. Boodi, N. Sudheer, A. P. Bidargaddi, S. Shatagar, and M. Telkar, "Semantic Segmentation of Computed Tomography Scan of Lungs," 2024 5th International Conference for Emerging Technology (INCET), Belgaum, India, 2024, pp. 1-7, doi: 10.1109/INCET61516.2024.10593534.

[22] F. Pasa et al., "Efficient Deep Network Architectures for Fast Chest X-Ray Tuberculosis Screening and Visualization," Scientific Reports, vol. 9, no. 1, p. 6268, Apr. 2019. doi: 10.1038/s41598-019-42557-4.

[23] E. Mique and A. Malicdem, "Deep Residual U-Net Based Lung Image Segmentation for Lung Disease Detection," IOP Conference Series: Materials Science and Engineering, vol. 803, no. 1, p. 012004, Apr. 2020. doi: 10.1088/1757-899X/803/1/012004.

[24] S. Gite, A. Mishra, and K. Kotecha, "Enhanced lung image segmentation using deep learning," Neural Computing and Applications, vol. 35, pp. 22839–22853, 2023. doi: 10.1007/s00521-021-06719-8